mathematics

MDPI

Article

Peak-to-Peak Stabilization of Sampled-Data Systems Subject to Actuator Saturation and Its Practical Application to an Inverted Pendulum

Khanh Hieu Nguyen and Sung Hyun Kim *

Department of Electrical, Electronic and Computer Engineering, University of Ulsan, Daehak-ro 93, Nam-gu, Ulsan 680-749, Republic of Korea; khanhhieutdh@ulsan.ac.kr

* Correspondence: shnkim@ulsan.ac.kr

Abstract: This paper investigates the local stability and stabilization criteria of sampled-data control systems, taking into account actuator saturation and peak-bounded exogenous disturbances. Specifically, this study introduces two innovations to extend the maximum upper bound of the sampling interval: two novel time integrals of the weighted state derivative are introduced to formulate an improved looped-functional; second, the introduction of two supplementary zero-equalities to improve the relationship among the components of the augmented state. Building on this, a set of linear matrix inequality-based stabilization conditions is derived. These conditions ensure that a closed-loop sampled-data system can become exponentially stable and achieve a guaranteed peak-to-peak performance in the domain of attraction. Finally, the efficacy of the proposed methodology is substantiated through both simulation and experimental results, focusing on the sampled-data control of an inverted pendulum system.

Keywords: sampled-data control; peak-to-peak performance; actuator saturation; inverted pendulum system

MSC: 93-08

Citation: Nguyen, K.H.; Kim, S.H. Peak-to-Peak Stabilization of Sampled-Data Systems Subject to Actuator Saturation and Its Practical Application to an Inverted Pendulum. *Mathematics* **2023**, *11*, 4592. https://doi.org/10.3390/math11224592

Academic Editors: Fangzheng Gao and Zhongcai Zhang

Received: 16 October 2023
Revised: 2 November 2023
Accepted: 7 November 2023
Published: 9 November 2023

1. Introduction

With the advancement of embedded systems, sampled-data systems (SDSs) have gained significant attention in the field of control due to their advantages of reliability, accuracy, ease of installation, and maintenance (refer to [1–4]). In this particular domain, numerous studies have focused on developing stability and stabilization criteria to extend the maximum upper bound of sampling interval, which can help reduce the computational burden and communication capacity. Specifically, ref. [5] proposed an input-delay model that characterizes SDSs as a class of continuous-time systems with time-delayed control inputs. Building on this model, ref. [6] explored a looped-functional that is not restricted to the positivity constraint, thereby offering the potential to relax the stability and stabilization criteria of the SDSs. Subsequently, ref. [7] introduced a two-sided looped function that can account for the system state information between two consecutive sampling times. Recently, ref. [8] extended this framework by including a zero integral function in the stability analysis process, while ref. [9] introduced novel discontinuous terms to relax the positive definiteness of the Lyapunov function. Furthermore, by considering single and double integrals for the state equation over the sampling interval, two previous papers [8,9] derived four zero-equalities with slack variables, facilitating the derivation of more flexible stability conditions. However, the methods in [7–9] still have the potential for improvement, as further system dynamics information associated with the sampling behavior can be effectively incorporated into the two-sided looped-functional. Moreover, the aforementioned zero-equalities are formulated in a bilinear form, which restricts their

direct applicability in deriving linear matrix inequality (LMI)-based stabilization conditions for SDSs.

Meanwhile, numerous intensive studies have been conducted on the control problem of inverted pendulum systems (IPSs) due to their wide application in various engineering fields, including humanoid robots, aerospace engineering, and personal transportation devices (refer to [10–14]). It is important to note that IPSs, being mechanical systems, are inevitably influenced by persistent peak-bounded disturbances caused by external factors such as friction, vibrations, or shaking. However, as in [15–18], the majority of the sampled-data control techniques, designed using a loop functional approach, have mainly focused on attenuating the effects of energy-bounded disturbances while ensuring a guaranteed $\mathcal{H}_\infty$ performance. To deal with the problem of peak-bounded disturbances, as demonstrated in [19,20], is to consider the peak-to-peak performance, which allows for analyzing the ratio of the peak performance output to the peak disturbance input. Additionally, it is crucial to consider the control saturation problem when designing a sampled-data control system, taking into account the limitations of real actuators and power supplies (see [21–24]). However, there is currently a lack of specific research achievements in the design of saturated sampled-data controllers for IPSs that ensure a guaranteed peak-to-peak performance.

Based on the aforementioned discussion, this paper aims to develop a method that can (1) extend the maximum upper bound of the sampling interval for sampled-data control systems, (2) ensure a guaranteed peak-to-peak performance, and (3) maintain the constraint of actuator saturation. Furthermore, experimental verification of the proposed method is conducted by applying it to the sampled-data control synthesis problem of an actual IPS. Consequently, the significant contributions of this paper toward less conservative stabilization conditions and results can be highlighted as follows:

- Note that the current time can be represented as two consecutive sampling times by utilizing additional time-varying parameters. By introducing two novel time integrals of the weighted state derivative, this paper makes the initial attempt to incorporate these parameters into the augmented state. This inclusion enables the utilization of the sawtooth-type characteristics of time-varying parameters during the stability analysis process. Furthermore, the proposed time integrals of the weighted state derivative play a crucial role in constructing an improved looped-functional that can contain a greater amount of system state information between two consecutive sampling times.
- In contrast to [8,9,15], this paper provides two additional zero-equalities that can improve the relationship among components of the augmented state, resulting in less conservative stabilization conditions. By reducing the number of zero-equalities, the proposed method offers the advantage of lowering the overall computational complexity owing to the utilization of fewer slack variables.
- In contrast to other existing studies that address the stabilization problem of SDSs with energy-bounded disturbances, this paper presents a set of stabilization conditions based on linear matrix inequalities (LMIs). These conditions ensure that the closed-loop sampled-data system achieves exponential stability and guarantees a peak-to-peak performance within the domain of attraction (DoA). Additionally, to design a practical sampled-data controller for IPSs, the actuator saturation constraint is also considered in this paper.

The remaining sections of this paper are structured as follows: Section 2 presents the objective of this paper. Section 3 provides the criteria for stability and stabilization. Section 4 demonstrates the application of the proposed method to an IPS. Finally, the contributions and achievements of this paper are summarized in Section 5.

Notations: Throughout this paper, $\mathbb{N}$ denotes the set of non-negative integers, $\mathbb{R}^n$ is the n-dimensional Euclidean space, and $\mathbb{R}^{n\times m}$ indicates the set of all $n \times m$ real matrixes. For a square matrix $\mathcal{Q} \in \mathbb{R}^{n\times m}$, the notation $\mathcal{Q} > 0$ means that $\mathcal{Q}$ is positive definite, $\mathcal{Q} \geq 0$ means that $\mathcal{Q}$ is positive semi-definite, $\mathrm{He}\{\mathcal{Q}\}$ indicates $\mathcal{Q} + \mathcal{Q}^T$, $\mathcal{Q}^T$ and $\mathcal{Q}^{-1}$ represent the transpose and inverse of $\mathcal{Q}$, respectively. The notation $(*)$ represents terms

induced by symmetry in symmetric block matrixes, and $\otimes$ denotes the Kronecker product. The function trace$(\cdot)$ returns the sum of diagonal matrix elements, sign$(\cdot)$ gives the argument sign, $\lambda_{\min}(\cdot)$ and $\lambda_{\max}(\cdot)$ return the minimum and maximum matrix eigenvalues, respectively. The notation diag$\{\cdot\}$ stands for the block-diagonal matrix, col$\{\cdot\}$ represents the column matrix, $0_{n\times m}$ denotes $n \times m$ null matrix, and I_n represents the $n \times n$ identity matrix. For any positive definite matrix $P \in \mathbb{R}^{n\times n}$ and vector $x(t)$, the set $\mathcal{E}(P,1) = \{x(t) \in \mathbb{R}^n \mid x^T(t)Px(t) \leq 1\}$ represents an ellipsoid in $\mathbb{R}^n$; the peak norm stands for $||w(t)||_\infty = \sup_{t\geq 0} ||w(t)||$, where $||w(t)||$ is the Euclidean norm of $w(t)$; and $\mathcal{L}_\infty^\omega = \{w(t) \in \mathbb{R}^\omega \mid ||w(t)||_\infty < \infty\}$.

2. Problem Formulation

Let us consider the following continuous-time linear systems:

$$\begin{cases} \dot{x}(t) = Ax(t) + Bu(t) + Ew(t) \\ z(t) = Cx(t) \end{cases} \tag{1}$$

where vectors $x(t) \in \mathbb{R}^n$, $u(t) \in \mathbb{R}^m$, $z(t) \in \mathbb{R}^v$, and $w(t) \in \mathcal{L}_\infty^\omega$ indicate the system state, the control input, the performance output, and the exogenous disturbances with a known peak norm $\bar{w}$, i.e., $||w(t)||_\infty = \bar{w}$, respectively; $A \in \mathbb{R}^{n\times n}$, $B \in \mathbb{R}^{n\times m}$, $C \in \mathbb{R}^{v\times n}$, and $E \in \mathbb{R}^{n\times\omega}$ are given system matrixes. In particular, as shown in Figure 1, the system state is measured at discrete sampling time t_k such that $t_0 = 0$ and $t_k < t_{k+1}$. Furthermore, sampling interval $h_k = t_{k+1} - t_k$ satisfies that

$$0 < h_k \in [h_m,\ h_M],\ \forall k \in \mathbb{N} \tag{2}$$

where h_m and h_M are the lower and upper bounds of the sampling interval.

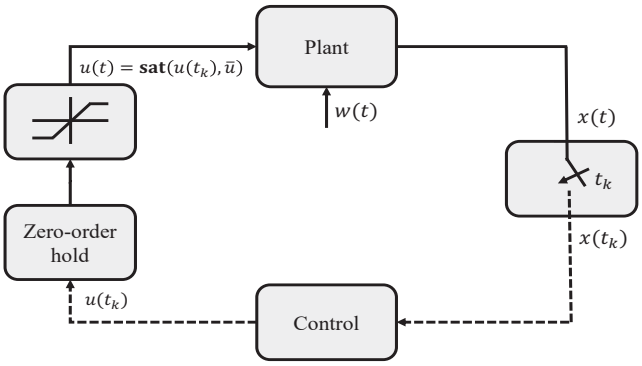

Figure 1. Sampled-data control systems with actuator saturation.

Additionally, this paper considers sampled-data control with respect to the following actuator saturation:

$$u(t) = \text{sat}\{u(t_k), \bar{u}\},\ t \in [t_k, t_{k+1}) \tag{3}$$

where $u(t_k) \in \mathbb{R}^m$ indicates the sampled-data control input; $\bar{u} \in \mathbb{R}^m$ denotes the saturation level; and the ℓth element of $u(t)$ is given by

$$u_\ell(t) = \text{sign}(u_\ell(t_k)) \times \min\{u_\ell(t_k), \bar{u}_\ell\},\ \forall \ell \in \{1, 2, \cdots, m\}$$

in which $u_\ell(t_k)$ and $\bar{u}_\ell$ represent the ℓth element of $u(t_k)$ and $\bar{u}$, respectively. Furthermore, according to Theorem 1 in [25], if there exists an auxiliary control input $v(t_k)$ subject to $|v(t_k)| \leq \bar{u}$, then (3) can be rewritten as follows:

$$u(t) = \sum_{i=1}^{2^m} \phi_i(t_k)\big(\Xi_i u(t_k) + \bar{\Xi}_i v(t_k)\big),\ t \in [t_k, t_{k+1}) \tag{4}$$

where Ξ_i and $\bar{\Xi}_i = I_m - \Xi_i$ belong to the set of $m \times m$ diagonal matrixes whose diagonal elements are either 1 or 0, and $\phi_i(t_k)$ indicates the weighting function satisfying that

$$\sum_{i=1}^{2^m} \phi_i(t_k) = 1,\ 0 \leq \phi_i(t_k) \leq 1,\ \forall i \in \{1, 2, \cdots, 2^m\}. \tag{5}$$

Subsequently, let us employ the following control law:

$$u(t_k) = Fx(t_k),\ v(t_k) = Kx(t_k)$$

where $F \in \mathbb{R}^{m\times n}$ and $K \in \mathbb{R}^{m\times n}$ denote the control gains to be designed later. Then, the resultant closed-loop system is represented from (1) and (4) as follows:

$$\begin{cases} \dot{x}(t) &= Ax(t) + \sum_{i=1}^{2^m} \phi_i(t_k)\bar{B}_i x(t_k) + Ew(t) \\ z(t) &= Cx(t) \end{cases} \tag{6}$$

subject to

$$x(t_k) \in \mathfrak{L}(K, \bar{u}) = \Big\{ x(t_k) \in \mathbb{R}^n \ \big|\ |Kx(t_k)| \leq \bar{u} \Big\} \tag{7}$$

where $\bar{B}_i = B(\Xi_i F + \bar{\Xi}_i K)$.

The objective of this paper is to design the sampled-data controller (4) that satisfies both of the following requirements (refer to [19,20]):

1. System (6) is exponentially stable in the absence of disturbances $w(t) \equiv 0$.
2. For a prescribed scalar $\gamma > 0$, an initial condition $x(t_0) = 0$, and any non-zero disturbances $w(t) \in \mathcal{L}_\infty^\varpi$, the performance output $z(t)$ satisfies

$$||z(t)||_\infty^2 - \gamma^2 ||w(t)||_\infty^2 < 0. \tag{8}$$

The following free-matrix-based integral inequality is utilized to address the single-integral quadratic terms arising from the time-derivative of looped-functional.

Lemma 1 ([26]). *For a differentiable function $x(t) \in \mathbb{R}^n$ for all $t \in [\alpha,\ \beta]$, and a matrix $0 < R = R^T \in \mathbb{R}^{n\times n}$, there exits matrixes $X \in \mathbb{R}^{n\times 3n}$ and $Y \in \mathbb{R}^{n\times 3n}$ such that the following condition holds:*

$$\begin{aligned} -\int_\alpha^\beta \dot{x}^T(\varphi) R \dot{x}(\varphi) d\varphi \leq (\beta-\alpha)\Big(\vartheta^T \Phi \vartheta - 2\big(x^T(\beta) + x^T(\alpha)\big) Y \vartheta\Big) \\ + 2\Big(\big(x^T(\beta) - x^T(\alpha)\big) X + 2\int_\alpha^\beta x^T(\varphi) d\varphi Y\Big)\vartheta \end{aligned}$$

where $\vartheta = col\Big\{x(\beta),\ x(\alpha),\ \int_\alpha^\beta x(\varphi)d\varphi\Big\} \in \mathbb{R}^{3n}$, $\Phi = X^T R^{-1} X + \frac{(\beta-\alpha)^2}{3} Y^T R^{-1} Y$.

3. Main Results

Let us designate $d_1(t) = t - t_k$ and $d_2(t) = t_{k+1} - t$, Then, the following block entry matrixes and augmented state will be utilized in the process of obtaining the stability and stabilization criteria:

$$\begin{aligned}
\mathbf{e}_p &= \begin{bmatrix} 0_{n\times(p-1)n} & I_n & 0_{n\times(8-p)n} \end{bmatrix} \in \mathbb{R}^{n\times 8n},\ \forall p \in \{1,\cdots,8\} \\
\vartheta(t) &= \operatorname{col}\Big\{ x(t),\ x(t_k),\ x(t_{k+1}),\ \int_{t_k}^{t} x(\varphi)d\varphi,\ \int_{t}^{t_{k+1}} x(\varphi)d\varphi, \\
&\qquad \int_{t_k}^{t} d_1(\varphi)\dot{x}(\varphi)d\varphi,\ \int_{t}^{t_{k+1}} d_2(\varphi)\dot{x}(\varphi)d\varphi,\ \dot{x}(t) \Big\} \in \mathbb{R}^{8n}
\end{aligned} \tag{9}$$

and the following vectors will be used for brevity:

$$\begin{aligned}
&\vartheta_1(t) = \Gamma_1\vartheta(t) \in \mathbb{R}^{5n},\ \dot{\vartheta}_1(t) = \bar{\Gamma}_1\vartheta(t),\ \vartheta_2(t) = \Gamma_2\vartheta(t) \in \mathbb{R}^{2n},\ \dot{\vartheta}_2(t) = \bar{\Gamma}_2\vartheta(t) \\
&\vartheta_3(t) = \Gamma_3\vartheta(t) \in \mathbb{R}^{2n},\ \dot{\vartheta}_3(t) = \bar{\Gamma}_3\vartheta(t),\ \vartheta_4(t) = \begin{bmatrix} \Gamma_2 \\ \mathbf{e}_6 \end{bmatrix}\vartheta(t) \in \mathbb{R}^{3n} \\
&\dot{\vartheta}_4(t) = \begin{bmatrix} \bar{\Gamma}_2 \\ d_1(t)\mathbf{e}_8 \end{bmatrix}\vartheta(t),\ \vartheta_5(t) = \begin{bmatrix} \Gamma_3 \\ \mathbf{e}_7 \end{bmatrix}\vartheta(t),\ \dot{\vartheta}_5(t) = \begin{bmatrix} \bar{\Gamma}_3 \\ -d_2(t)\mathbf{e}_8 \end{bmatrix}\vartheta(t) \in \mathbb{R}^{3n} \\
&\vartheta_6(t) = \Gamma_6\vartheta(t),\ \vartheta_7(t) = \Gamma_7\vartheta(t) \in \mathbb{R}^{3n}
\end{aligned}$$

where

$$\begin{aligned}
&\Gamma_1^T = \begin{bmatrix} \mathbf{e}_1^T & \mathbf{e}_2^T & \mathbf{e}_3^T & \mathbf{e}_4^T & \mathbf{e}_5^T \end{bmatrix},\ \bar{\Gamma}_1^T = \begin{bmatrix} \mathbf{e}_8^T & 0 & 0 & \mathbf{e}_1^T & -\mathbf{e}_1^T \end{bmatrix} \\
&\Gamma_2^T = \begin{bmatrix} \mathbf{e}_1^T - \mathbf{e}_2^T & \mathbf{e}_4^T \end{bmatrix},\ \bar{\Gamma}_2^T = \begin{bmatrix} \mathbf{e}_8^T & \mathbf{e}_1^T \end{bmatrix},\ \Gamma_3^T = \begin{bmatrix} \mathbf{e}_3^T - \mathbf{e}_1^T & \mathbf{e}_5^T \end{bmatrix} \\
&\bar{\Gamma}_3^T = \begin{bmatrix} -\mathbf{e}_8^T & -\mathbf{e}_1^T \end{bmatrix},\ \Gamma_6^T = \begin{bmatrix} \mathbf{e}_1^T & \mathbf{e}_2^T & \mathbf{e}_4^T \end{bmatrix},\ \Gamma_7^T = \begin{bmatrix} \mathbf{e}_1^T & \mathbf{e}_3^T & \mathbf{e}_5^T \end{bmatrix}.
\end{aligned}$$

Remark 1. *In contrast to [8,9,15], this paper constructs two novel time integrals of the weighted state derivative, i.e., $\int_{t_k}^{t} d_1(\varphi)\dot{x}(\varphi)d\varphi$ and $\int_{t}^{t_{k+1}} d_2(\varphi)\dot{x}(\varphi)d\varphi$. Accordingly, more additional information about (i) the sawtooth-type characteristics of the time-varying parameters $d_1(t)$ and $d_2(t)$ and (ii) the system state between two consecutive sampling times can be used to derive less conservative stability and stabilization criteria.*

3.1. Stability Analysis

Now, let us establish the following Lyapunov functional-based candidate:

$$V(t) = \sum_{\ell=1}^{4} V_\ell(t),\ \text{for } t \in [t_k, t_{k+1}) \tag{10}$$

where

$$\begin{aligned}
V_1(t) &= x^T(t)Px(t) \\
V_2(t) &= 2\vartheta_1^T(t)\big(d_2(t)W_1\vartheta_2(t) + d_1(t)W_2\vartheta_3(t)\big) \\
V_3(t) &= 2\vartheta_4^T(t)S(t)\vartheta_5(t) \\
V_4(t) &= d_2(t)\int_{t_k}^{t} e^{\sigma(\varphi-t)}\dot{x}^T(\varphi)R_1\dot{x}(\varphi)d\varphi - d_1(t)\int_{t}^{t_{k+1}} e^{\sigma(\varphi-t)}\dot{x}^T(\varphi)R_2\dot{x}(\varphi)d\varphi
\end{aligned}$$

with $0 < P = P^T \in \mathbb{R}^{n\times n}$, $W_1, W_2 \in \mathbb{R}^{5n\times 2n}$,

$$S(t) = \begin{bmatrix} d_1(t)S_1 + d_2(t)S_2 & S_3 \\ S_4 & S_5 \end{bmatrix} \in \mathbb{R}^{3n\times 3n}$$

$S_1, S_2 \in \mathbb{R}^{2n\times 2n}$, $S_3 \in \mathbb{R}^{2n\times n}$, $S_4 \in \mathbb{R}^{n\times 2n}$, $S_5 \in \mathbb{R}^{n\times n}$, $R_1 = R_1^T$, and $R_2 = R_2^T \in \mathbb{R}^{n\times n}$.

Remark 2. *It is worth noting that $\vartheta_2(t) = 0$ and $\vartheta_4(t) = 0$ at $t = t_k$, and $\vartheta_3(t) = 0$ and $\vartheta_5(t) = 0$ at $t = t_{k+1}$. Thus, it is clear that $V(t_k) = V_1(t_k)$, for all $k \in \mathbb{N}$. Accordingly, the positive definiteness requirement of $V_2(t)$, $V_3(t)$, and $V_4(t)$ can be excluded based on the looped-functional approach [6].*

Lemma 2 offers the fundamental peak-to-peak stability criteria for sampled-data control systems subject to actuator saturation.

Lemma 2. *For given positive scalars σ, γ, and $\bar{u}$, system (6) subject to (7) is exponentially stable with a guaranteed peak-to-peak performance γ in the DoA $\mathcal{E}(P,1)$, if the following conditions hold:*

$$0 > \dot{V}(t) + \sigma V(t) + ||z(t)||^2 - \gamma^2||w(t)||^2 \tag{11}$$

$$\mathcal{E}\left(P, 1 + \frac{\gamma^2}{\sigma}\bar{w}^2\right) \subset \mathfrak{L}(K,\bar{u}). \tag{12}$$

Proof of Lemma 2. *(Local stability)* By multiplying (11) by $e^{\sigma t}$ and integrating it over $[t_k, t_{k+1})$, we have

$$V(t_{k+1}) < e^{\sigma(t_k - t_{k+1})}V(t_k) - \int_{t_k}^{t_{k+1}} e^{\sigma(\varphi - t_{k+1})}||z(\varphi)||^2 d\varphi + \gamma^2 \int_{t_k}^{t_{k+1}} e^{\sigma(\varphi - t_{k+1})}||w(\varphi)||^2 d\varphi$$

which leads to

$$\begin{aligned} V(t_k) &< e^{\sigma(t_{k-1} - t_k)}V(t_{k-1}) - \int_{t_{k-1}}^{t_k} e^{\sigma(\varphi - t_k)}||z(\varphi)||^2 d\varphi + \gamma^2 \int_{t_{k-1}}^{t_k} e^{\sigma(\varphi - t_k)}||w(\varphi)||^2 d\varphi \\ &< \cdots \\ &< e^{-\sigma t_k}V(t_0) - \int_{t_0}^{t_k} e^{\sigma(\varphi - t_k)}||z(\varphi)||^2 d\varphi + \gamma^2 \int_{t_0}^{t_k} e^{\sigma(\varphi - t_k)}||w(\varphi)||^2 d\varphi, \ \forall k \in \mathbb{N}. \end{aligned} \tag{13}$$

Thus, for $w(t) \equiv 0$, it follows from (13) that

$$||x(t_k)||^2 < e^{-\sigma t_k}\frac{\lambda_{\max}(P)}{\lambda_{\min}(P)}||x(t_0)||^2, \ \forall k \in \mathbb{N} \tag{14}$$

which means that system (6) is exponentially stable.

Next, let us consider an initial condition $x(t_0) \in \mathcal{E}(P,1)$. Then, since $||w(t)||_\infty^2 = \bar{w}^2$, condition (13) implies

$$\begin{aligned} V(t_k) &< \sup_{k\in\mathbb{N}}\left\{e^{-\sigma t_k}V(t_0) - \int_{t_0}^{t_k} e^{\sigma(\varphi - t_k)}||z(\varphi)||^2 d\varphi + \gamma^2 \int_{t_0}^{t_k} e^{\sigma(\varphi - t_k)}||w(\varphi)||^2 d\varphi\right\} \\ &\le V(t_0) - ||z(t)||_\infty^2 \cdot \sup_{k\in\mathbb{N}}\left\{\int_{t_0}^{t_k} e^{\sigma(\varphi - t_k)}d\varphi\right\} + \gamma^2||w(t)||_\infty^2 \cdot \sup_{k\in\mathbb{N}}\left\{\int_{t_0}^{t_k} e^{\sigma(\varphi - t_k)}d\varphi\right\} \\ &\le 1 + \frac{\gamma^2}{\sigma}\bar{w}^2, \ \forall k \in \mathbb{N}. \end{aligned} \tag{15}$$

Accordingly, by (12) and (15), it is obtained that

$$x(t_k) \in \mathcal{E}\left(P, 1 + \frac{\gamma^2}{\sigma}\bar{w}^2\right) \subset \mathfrak{L}(K,\bar{u}), \ \forall k \in \mathbb{N} \tag{16}$$

which means that (7) is ensured despite the presence of peak-bounded disturbances.

(Peak-to-peak performance) For $x(t_0) \equiv 0$, it follows from (15) that

$$\sigma V(t_k) < -||z(t)||_\infty^2 + \gamma^2 ||w(t)||_\infty^2, \ \forall k \in \mathbb{N}. \tag{17}$$

Therefore, since $V(t_k) = V_1(t_k) > 0$, it is satisfied by (17) that

$$||z(t)||_\infty^2 - \gamma^2 ||w(t)||_\infty^2 < 0 \tag{18}$$

which corresponds to (8) with a guaranteed peak-to-peak performance γ for all nonzero peak-bounded disturbances. □

Then, Lemma 3 provides a set of LMIs for stability conditions (11) and (12).

Lemma 3. *For given positive scalars σ, γ, h_m, h_M, and $\bar{u}$, system (6) subject to (7) is exponentially stable with a guaranteed peak-to-peak performance γ in the DoA $\mathcal{E}(P,1)$, if there exist positive definite matrixes $P \in \mathbb{R}^{n\times n}$, R_1, $R_2 \in \mathbb{R}^{n\times n}$, any matrixes $G \in \mathbb{R}^{n\times 8n}$, W_1, $W_2 \in \mathbb{R}^{5n\times 2n}$, S_1, $S_2 \in \mathbb{R}^{2n\times 2n}$, $S_3 \in \mathbb{R}^{2n\times n}$, $S_4 \in \mathbb{R}^{n\times 2n}$, $S_5 \in \mathbb{R}^{n\times n}$, X_1, $X_2 \in \mathbb{R}^{n\times 3n}$, Y_1, $Y_2 \in \mathbb{R}^{n\times 3n}$, and U_1, $U_2 \in \mathbb{R}^{n\times 8n}$, such that for $h \in \{h_m,\ h_M\}$, $q \in \{1,2\}$, and $i \in \{1,2,\cdots,2^m\}$, the following conditions hold:*

$$0 > \begin{bmatrix} \Psi_i^* + \Psi_0 + h\Psi_q & (*) & (*) & (*) \\ E^T G & -\gamma^2 I & 0 & 0 \\ C\mathbf{e}_1 & 0 & -I & 0 \\ h\mathcal{X}_q & 0 & 0 & -h\mathcal{R}_q \end{bmatrix} \tag{19}$$

$$0 \le \begin{bmatrix} P & (*) \\ \Lambda_\ell K & \eta_\ell \end{bmatrix}, \ \forall \ell \in \{1,2,\cdots,m\} \tag{20}$$

where

$$\begin{aligned}
\Psi_i^* &= He\{G^T(-\mathbf{e}_8 + A\mathbf{e}_1 + \bar{B}_i\mathbf{e}_2)\} \\
\Psi_0 &= He\{\mathbf{e}_1^T P\mathbf{e}_8 - \Gamma_1^T W_1\Gamma_2 + \Gamma_1^T W_2\Gamma_3 + \Gamma_2^T(S_1 - S_2)\Gamma_3 + \bar{\Gamma}_2^T S_3\mathbf{e}_7 + \mathbf{e}_6^T S_4\bar{\Gamma}_3 \\
&\quad + e^{-\sigma h_M}\big((\mathbf{e}_1^T - \mathbf{e}_2^T)X_1 + 2\mathbf{e}_4^T Y_1\big)\Gamma_6 + \big((\mathbf{e}_3^T - \mathbf{e}_1^T)X_2 + 2\mathbf{e}_5^T Y_2\big)\Gamma_7 \\
&\quad - (\mathbf{e}_4^T + \mathbf{e}_6^T)U_1 - (\mathbf{e}_5^T - \mathbf{e}_7^T)U_2 + \Gamma_2^T\sigma S_3\mathbf{e}_7 + \mathbf{e}_6^T\sigma S_4\Gamma_3 + \mathbf{e}_6^T\sigma S_5\mathbf{e}_7\} + \mathbf{e}_1^T\sigma P\mathbf{e}_1 \\
\Psi_1 &= He\{\bar{\Gamma}_1^T W_2\Gamma_3 + \Gamma_1^T W_2\bar{\Gamma}_3 + \Gamma_1^T\sigma W_2\Gamma_3 + \Gamma_2^T\sigma S_1\Gamma_3 + \bar{\Gamma}_2^T S_1\Gamma_3 + \Gamma_2^T S_1\bar{\Gamma}_3 \\
&\quad + \mathbf{e}_8^T S_4\Gamma_3 + \mathbf{e}_8^T S_5\mathbf{e}_7 - e^{-\sigma h_M}(\mathbf{e}_1^T + \mathbf{e}_2^T)Y_1\Gamma_6 + \mathbf{e}_1^T U_1\} + \mathbf{e}_8^T R_2\mathbf{e}_8 \\
\Psi_2 &= He\{\bar{\Gamma}_1^T W_1\Gamma_2 + \Gamma_1^T W_1\bar{\Gamma}_2 + \Gamma_1^T\sigma W_1\Gamma_2 + \Gamma_2^T\sigma S_2\Gamma_3 + \bar{\Gamma}_2^T S_2\Gamma_3 + \Gamma_2^T S_2\bar{\Gamma}_3 \\
&\quad - \Gamma_2^T S_3\mathbf{e}_8 - \mathbf{e}_6^T S_5\mathbf{e}_8 - (\mathbf{e}_3^T + \mathbf{e}_1^T)Y_2\Gamma_7 + \mathbf{e}_1^T U_2\} + \mathbf{e}_8^T R_1\mathbf{e}_8 \\
\mathcal{X}_1 &= col\{X_1\Gamma_6,\ h_M Y_1\Gamma_6\},\ \mathcal{R}_1 = e^{\sigma h_M} diag\{R_1,\ 3R_1\} \\
\mathcal{X}_2 &= col\{X_2\Gamma_7,\ h_M Y_2\Gamma_7\},\ \mathcal{R}_2 = diag\{R_2,\ 3R_2\} \\
\Lambda_\ell &= \begin{bmatrix} 0_{1\times(\ell-1)} & 1 & 0_{1\times(m-\ell)} \end{bmatrix},\ \eta_\ell = \frac{\bar{u}_\ell^2}{1 + \frac{\gamma^2}{\sigma}\bar{w}^2}.
\end{aligned}$$

Proof of Lemma 3. The time derivatives of (10) are given as follows:

$$\dot{V}_1(t) = 2\vartheta^T(t)\mathbf{e}_1^T P\mathbf{e}_8\vartheta(t) \tag{21}$$

$$\begin{aligned}
\dot{V}_2(t) &= 2\vartheta^T(t)\Big(-\Gamma_1^T W_1\Gamma_2 + \Gamma_1^T W_2\Gamma_3 + d_2(t)\big(\bar{\Gamma}_1^T W_1\Gamma_2 + \Gamma_1^T W_1\bar{\Gamma}_2\big) \\
&\quad + d_1(t)\big(\bar{\Gamma}_1^T W_2\Gamma_3 + \Gamma_1^T W_2\bar{\Gamma}_3\big)\Big)\vartheta(t)
\end{aligned} \tag{22}$$

$$\begin{aligned}\dot{V}_3(t) &= 2\vartheta^T(t)\Big(\Gamma_2^T(S_1-S_2)\Gamma_3+\bar{\Gamma}_2^T S_3\mathbf{e}_7+\mathbf{e}_6^T S_4\bar{\Gamma}_3\\ &\quad+d_1(t)\big(\bar{\Gamma}_2^T S_1\Gamma_3+\Gamma_2^T S_1\bar{\Gamma}_3+\mathbf{e}_8^T S_4\Gamma_3+\mathbf{e}_8^T S_5\mathbf{e}_7\big)\\ &\quad+d_2(t)\big(\bar{\Gamma}_2^T S_2\Gamma_3+\Gamma_2^T S_2\bar{\Gamma}_3-\Gamma_2^T S_3\mathbf{e}_8-\mathbf{e}_6^T S_5\mathbf{e}_8\big)\Big)\vartheta(t) \qquad (23)\\ \dot{V}_4(t) &= \vartheta^T(t)\Big(d_2(t)\mathbf{e}_8^T R_1\mathbf{e}_8+d_1(t)\mathbf{e}_8^T R_2\mathbf{e}_8\Big)\vartheta(t)\\ &\quad-\sigma d_2(t)\int_{t_k}^{t}e^{\sigma(\varphi-t)}\dot{x}^T(\varphi)R_1\dot{x}(\varphi)d\varphi-\underbrace{\int_{t_k}^{t}e^{\sigma(\varphi-t)}\dot{x}^T(\varphi)R_1\dot{x}(\varphi)d\varphi}_{(\mathbf{a})}\\ &\quad+\sigma d_1(t)\int_{t}^{t_{k+1}}e^{\sigma(\varphi-t)}\dot{x}^T(\varphi)R_2\dot{x}(\varphi)d\varphi-\underbrace{\int_{t}^{t_{k+1}}e^{\sigma(\varphi-t)}\dot{x}^T(\varphi)R_2\dot{x}(\varphi)d\varphi}_{(\mathbf{b})}. \qquad (24)\end{aligned}$$

Additionally, it is worth noting that

$$\sigma V_1(t) = \vartheta^T(t)\mathbf{e}_1^T\sigma P\mathbf{e}_1\vartheta(t) \qquad (25)$$

$$\sigma V_2(t) = 2\vartheta^T(t)\big(d_2(t)\Gamma_1^T\sigma W_1\Gamma_2+d_1(t)\Gamma_1^T\sigma W_2\Gamma_3\big)\vartheta(t) \qquad (26)$$

$$\sigma V_3(t) = 2\vartheta^T(t)\big(d_1(t)\Gamma_2^T\sigma S_1\Gamma_3+d_2(t)\Gamma_2^T\sigma S_2\Gamma_3+\Gamma_2^T\sigma S_3\mathbf{e}_7+\mathbf{e}_6^T\sigma S_4\Gamma_3+\mathbf{e}_6^T\sigma S_5\mathbf{e}_7\big)\vartheta(t) \qquad (27)$$

$$\sigma V_4(t) = \sigma d_2(t)\int_{t_k}^{t}e^{\sigma(\varphi-t)}\dot{x}^T(\varphi)R_1\dot{x}(\varphi)d\varphi-\sigma d_1(t)\int_{t}^{t_{k+1}}e^{\sigma(\varphi-t)}\dot{x}^T(\varphi)R_2\dot{x}(\varphi)d\varphi. \qquad (28)$$

Furthermore, from

$$\begin{aligned}\int_{t_k}^{t}d_1(t)\dot{x}(\varphi)d\varphi &= d_1(t)x(t)-\int_{t_k}^{t}x(\varphi)d\varphi\\ \int_{t}^{t_{k+1}}d_2(t)\dot{x}(\varphi)d\varphi &= -d_2(t)x(t)+\int_{t}^{t_{k+1}}x(\varphi)d\varphi\end{aligned}$$

two additional zero-equalities are given as follows:

$$0 = 2\vartheta^T(t)\Big(d_1(t)\mathbf{e}_1^T-\mathbf{e}_4^T-\mathbf{e}_6^T\Big)U_1\vartheta(t) \qquad (29)$$

$$0 = 2\vartheta^T(t)\Big(d_2(t)\mathbf{e}_1^T-\mathbf{e}_5^T+\mathbf{e}_7^T\Big)U_2\vartheta(t). \qquad (30)$$

Also, from (6), it follows that

$$0 = 2\vartheta^T(t)G^T\Big(-\mathbf{e}_8+A\mathbf{e}_1+\sum_{i=1}^{2^m}\phi_i(t_k)\bar{B}_i\mathbf{e}_2\Big)\vartheta(t)+2\vartheta^T(t)G^TEw(t). \qquad (31)$$

In particular, based on (2), Lemma 1 allows

$$\begin{aligned}(\mathbf{a}) &\le -e^{-\sigma h_M}\int_{t_k}^{t}\dot{x}^T(\varphi)R_1\dot{x}(\varphi)d\varphi\\ &\le \vartheta^T(t)e^{-\sigma h_M}\Big(d_1(t)\big(\Gamma_6^T\Phi_1\Gamma_6-2(\mathbf{e}_1^T+\mathbf{e}_2^T)Y_1\Gamma_6\big)+2\big((\mathbf{e}_1^T-\mathbf{e}_2^T)X_1+2\mathbf{e}_4^TY_1\big)\Gamma_6\Big)\vartheta(t) \qquad (32)\\ (\mathbf{b}) &\le \int_{t}^{t_{k+1}}\dot{x}^T(\varphi)R_2\dot{x}(\varphi)d\varphi\\ &\le \vartheta^T(t)\Big(d_2(t)\big(\Gamma_7^T\Phi_2\Gamma_7-2(\mathbf{e}_3^T+\mathbf{e}_1^T)Y_2\Gamma_7\big)+2\big((\mathbf{e}_3^T-\mathbf{e}_1^T)X_2+2\mathbf{e}_5^TY_2\big)\Gamma_7\Big)\vartheta(t) \qquad (33)\end{aligned}$$

where

$$\Phi_q = X_q^TR_q^{-1}X_q+\frac{h_M^2}{3}Y_q^TR_q^{-1}Y_q,\ \forall q\in\{1,2\}.$$

Thus, by combining (21)–(31), and applying (32) and (33), we have

$$\dot{V}(t) + \sigma V(t) + ||z(t)||^2 - \gamma^2 ||w(t)||^2 \leq \sum_{i=1}^{2^m} \phi_i(t_k) \bar{\vartheta}^T(t) \Theta_i \bar{\vartheta}(t) \tag{34}$$

where $\bar{\vartheta}(t) = \text{col}\{\vartheta(t), w(t)\} \in \mathbb{R}^{8n+\omega}$, $\Upsilon = \begin{bmatrix} I_{8n} & 0_{8n\times\omega} \end{bmatrix}$, and

$$\Theta_i = \begin{bmatrix} \Psi_i^* + \Psi_0 & (*) \\ E^T G & -\gamma^2 I \end{bmatrix} + \begin{bmatrix} \mathbf{e}_1^T C^T \\ 0 \end{bmatrix} \begin{bmatrix} C\mathbf{e}_1 & 0 \end{bmatrix} + \frac{d_1(t)}{h_k} h_k \Upsilon^T (\Psi_1 + e^{-\sigma h_M} \Gamma_6^T \Phi_1 \Gamma_6) \Upsilon + \frac{d_2(t)}{h_k} h_k \Upsilon^T (\Psi_2 + \Gamma_7^T \Phi_2 \Gamma_7) \Upsilon.$$

As a result, based on (5) and $\frac{d_1(t)}{h_k} + \frac{d_2(t)}{h_k} = 1$, condition (11) is ensured by the following conditions, for $h \in \{h_m, h_M\}$ and $i \in \{1, 2, \cdots, 2^m\}$:

$$0 > \begin{bmatrix} \Psi_i^* + \Psi_0 & (*) \\ E^T G & -\gamma^2 I \end{bmatrix} + \begin{bmatrix} \mathbf{e}_1^T C^T \\ 0 \end{bmatrix} \begin{bmatrix} C\mathbf{e}_1 & 0 \end{bmatrix} + h \Upsilon^T (\Psi_1 + e^{-\sigma h_M} \Gamma_6^T \Phi_1 \Gamma_6) \Upsilon \tag{35}$$

$$0 > \begin{bmatrix} \Psi_i^* + \Psi_0 & (*) \\ E^T G & -\gamma^2 I \end{bmatrix} + \begin{bmatrix} \mathbf{e}_1^T C^T \\ 0 \end{bmatrix} \begin{bmatrix} C\mathbf{e}_1 & 0 \end{bmatrix} + h \Upsilon^T (\Psi_2 + \Gamma_7^T \Phi_2 \Gamma_7) \Upsilon \tag{36}$$

which are converted into (19) by the Schur complement.

Next, the Schur complement of (20) yields

$$\frac{1}{1 + \frac{\gamma^2}{\sigma} \bar{w}^2} P \geq \frac{1}{\bar{u}_\ell^2} K^T \Lambda_\ell^T \bar{\Lambda}_\ell K, \ \forall \ell \in \{1, 2, \cdots, m\}$$

which implies that $\mathcal{E}\left(P, 1 + \frac{\gamma^2}{\sigma} \bar{w}^2\right) \subset \mathfrak{L}(K, \bar{u})$. □

Remark 3. *It should be noted that the zero-equalities in [8,9,15] cannot be directly applied to derive stabilization conditions of SDSs since they are formulated in bilinear form. To overcome these limitations, this paper provides two additional zero-equalities (29) and (30). These two zero-equalities enhance the relationship among the elements of $\vartheta(t)$ and can be utilized to derive stabilization conditions in a less conservative manner. Further, this paper adopts two fewer zero-equalitiesthan [8,9,15], which plays a key role in reducing the number of variables (NoVs).*

As a consequence of Lemma 3, Corollary 1 offers the LMI-based stability criteria for the sampled-data systems in the absence of disturbances

$$\dot{x}(t) = Ax(t) + A_s x(t_k), \text{ for } t \in [t_k, t_{k+1}), \ \forall k \in \mathbb{N} \tag{37}$$

where $A \in \mathbb{R}^{n\times n}$ and $A_s \in \mathbb{R}^{n\times n}$ are given system matrixes.

Corollary 1. *For given positive scalars σ, h_m, and h_M, system (37) is exponentially stable, if there exist positive definite matrixes $P \in \mathbb{R}^{n\times n}$, R_1, $R_2 \in \mathbb{R}^{n\times n}$, any matrixes $G \in \mathbb{R}^{n\times 8n}$, W_1, $W_2 \in \mathbb{R}^{5n\times 2n}$ S_1, $S_2 \in \mathbb{R}^{2n\times 2n}$, $S_3 \in \mathbb{R}^{2n\times n}$, $S_4 \in \mathbb{R}^{n\times 2n}$, $S_5 \in \mathbb{R}^{n\times n}$, X_1, $X_2 \in \mathbb{R}^{n\times 3n}$, Y_1, $Y_2 \in \mathbb{R}^{n\times 3n}$, and U_1, $U_2 \in \mathbb{R}^{n\times 8n}$, such that for $h \in \{h_m, h_M\}$ and $q \in \{1, 2\}$, the following conditions hold:*

$$0 > \begin{bmatrix} \Psi^* + \Psi_0 + h\Psi_q & (*) \\ h\mathcal{X}_q & -h\mathcal{R}_q \end{bmatrix} \tag{38}$$

in which Ψ_0, Ψ_q, $\mathcal{X}_p$, and $\mathcal{R}_p$ are defined in Lemma 3, and

$$\Psi^* = He\{G^T(-\mathbf{e}_8 + A\mathbf{e}_1 + A_s\mathbf{e}_2)\}.$$

Proof of Lemma 1. In the absence of disturbances and actuator saturation constraints, condition (34) can be reduced to

$$\dot{V}(t) + \sigma V(t) \leq \vartheta^T(t)\Theta\vartheta(t) \tag{39}$$

where

$$\Theta = \Psi^* + \Psi_0 + \frac{d_1(t)}{h_k}h_k\big(\Psi_1 + e^{-\sigma h_M}\Gamma_6^T\Phi_1\Gamma_6\big) + \frac{d_2(t)}{h_k}h_k\big(\Psi_2 + \Gamma_7^T\Phi_2\Gamma_7\big).$$

Thus, the exponential stability condition $\dot{V}(t) + \sigma V(t) < 0$ is equivalent to the following conditions, for $h \in \{h_m,\ h_M\}$:

$$0 > \Psi^* + \Psi_0 + h\big(\Psi_1 + e^{-\sigma h_M}\Gamma_6^T\Phi_1\Gamma_6\big) \tag{40}$$

$$0 > \Psi^* + \Psi_0 + h\big(\Psi_2 + \Gamma_7^T\Phi_2\Gamma_7\big) \tag{41}$$

which are converted into (38) by the Schur complement. □

Remark 4. *The NoVs required for Corollary 1 are* $70.5n^2 + 1.5n$. *On the other hand, the NoVs for Theorem 1 in [8], Corrollary 1 in [9], Theorem 3 in [15], are* $116.5n^2 + 4.5n$, $70.5n^2 + 4.5n$, *and* $111.5n^2 + 4.5n$, *respectively. Thus, it is clear that the proposed method requires a lower computational complexity than those of [8,9,15].*

3.2. Stabilization Criteria

Based on Lemma 3, Theorem 1 presents the peak-to-peak stabilization conditions for SDSs subject to actuator saturation, formulated in terms of LMIs.

Theorem 1. *For given positive scalars* σ, γ, χ_1, χ_2, μ, h_m, h_M, *and* $\bar{u}$, *system (6) subject to (7) is exponentially stable with a guaranteed peak-to-peak performance* γ *in the DoA* $\mathcal{E}(P,1)$, *if there exist positive definite matrixes* $\bar{P} \in \mathbb{R}^{n\times n}$, $\bar{R}_1$, $\bar{R}_2 \in \mathbb{R}^{n\times n}$, *any matrixes* $\bar{G} \in \mathbb{R}^{n\times n}$, $P_0 = P_0^T \in \mathbb{R}^{n\times n}$, W_1, $W_2 \in \mathbb{R}^{5n\times 2n}$, $\bar{S}_1$, $\bar{S}_2 \in \mathbb{R}^{2n\times 2n}$, $\bar{S}_3 \in \mathbb{R}^{2n\times n}$, $\bar{S}_4 \in \mathbb{R}^{n\times 2n}$, $\bar{S}_5 \in \mathbb{R}^{n\times n}$, $\bar{X}_1$, $\bar{X}_2 \in \mathbb{R}^{n\times 3n}$, $\bar{Y}_1$, $\bar{Y}_2 \in \mathbb{R}^{n\times 3n}$, $\bar{U}_1$, $\bar{U}_2 \in \mathbb{R}^{n\times 8n}$, $\bar{F} \in \mathbb{R}^{m\times n}$ *and* $\bar{K} \in \mathbb{R}^{m\times n}$, *such that for* $h \in \{h_m,\ h_M\}$, $q \in \{1,2\}$, *and* $i \in \{1,2,\cdots,2^m\}$, *the following conditions hold:*

$$0 > \begin{bmatrix} \bar{\Psi}_i^* + \bar{\Psi}_0 + h\bar{\Psi}_q & (*) & (*) & (*) \\ E^T\Gamma_8 & -\gamma^2 I & 0 & 0 \\ C\bar{G}\mathbf{e}_1 & 0 & -I & 0 \\ h\bar{\mathcal{X}}_q & 0 & 0 & -h\bar{\mathcal{R}}_q \end{bmatrix} \tag{42}$$

$$0 \leq \begin{bmatrix} \bar{P} & (*) \\ \Lambda_\ell\bar{K} & \eta_\ell \end{bmatrix},\ \forall \ell \in \{1,2,\cdots,m\} \tag{43}$$

$$0 \leq \begin{bmatrix} P_0 & \mu I \\ (*) & He\{\mu\bar{G}\} - \bar{P} \end{bmatrix} \tag{44}$$

where Λ_ℓ *and* η_ℓ *are given in Lemma 3, and*

$$\begin{aligned}
\bar{\Psi}_i^* &= He\Big\{\Gamma_8^T\big(-\bar{G}\mathbf{e}_8 + A\bar{G}\mathbf{e}_1 + B(\Xi_i\bar{F} + \bar{\Xi}_i\bar{K})\mathbf{e}_2\big)\Big\},\ \Gamma_8 = \mathbf{e}_1\chi_1 + \mathbf{e}_2\chi_2 + \mathbf{e}_8 \\
\bar{\Psi}_0 &= He\big\{\mathbf{e}_1^T\bar{P}\mathbf{e}_8 - \Gamma_1^T\bar{W}_1\Gamma_2 + \Gamma_1^T\bar{W}_2\Gamma_3 + \Gamma_2^T(\bar{S}_1 - \bar{S}_2)\Gamma_3 + \bar{\Gamma}_2^T\bar{S}_3\mathbf{e}_7 + \mathbf{e}_6^T\bar{S}_4\bar{\Gamma}_3 \\
&\quad + e^{-\sigma h_M}\big((\mathbf{e}_1^T - \mathbf{e}_2^T)\bar{X}_1 + 2\mathbf{e}_4^T\bar{Y}_1\big)\Gamma_6 + \big((\mathbf{e}_3^T - \mathbf{e}_1^T)\bar{X}_2 + 2\mathbf{e}_5^T\bar{Y}_2\big)\Gamma_7 \\
&\quad - (\mathbf{e}_4^T + \mathbf{e}_6^T)\bar{U}_1 - (\mathbf{e}_5^T - \mathbf{e}_7^T)\bar{U}_2 + \Gamma_2^T\sigma\bar{S}_3\mathbf{e}_7 + \mathbf{e}_6^T\sigma\bar{S}_4\Gamma_3 + \mathbf{e}_6^T\sigma\bar{S}_5\mathbf{e}_7\big\} + \mathbf{e}_1^T\sigma\bar{P}\mathbf{e}_1 \\
\bar{\Psi}_1 &= He\big\{\bar{\Gamma}_1^T\bar{W}_2\Gamma_3 + \Gamma_1^T\bar{W}_2\bar{\Gamma}_3 + \Gamma_1^T\sigma\bar{W}_2\Gamma_3 + \Gamma_2^T\sigma\bar{S}_1\Gamma_3 + \bar{\Gamma}_2^T\bar{S}_1\Gamma_3 + \Gamma_2^T\bar{S}_1\bar{\Gamma}_3 \\
&\quad + \mathbf{e}_8^T\bar{S}_4\Gamma_3 + \mathbf{e}_8^T\bar{S}_5\mathbf{e}_7 - e^{-\sigma h_M}(\mathbf{e}_1^T + \mathbf{e}_2^T)\bar{Y}_1\Gamma_6 + \mathbf{e}_1^T\bar{U}_1\big\} + \mathbf{e}_8^T\bar{R}_2\mathbf{e}_8
\end{aligned}$$

$$\begin{aligned}\bar{\Psi}_2 &= He\{\bar{\Gamma}_1^T\bar{W}_1\Gamma_2 + \Gamma_1^T\bar{W}_1\bar{\Gamma}_2 + \Gamma_1^T\sigma\bar{W}_1\Gamma_2 + \Gamma_2^T\sigma\bar{S}_2\Gamma_3 + \bar{\Gamma}_2^T\bar{S}_2\Gamma_3 + \Gamma_2^T\bar{S}_2\bar{\Gamma}_3\\ &\quad - \Gamma_2^T\bar{S}_3\mathbf{e}_8 - \mathbf{e}_6^T\bar{S}_5\mathbf{e}_8 - (\mathbf{e}_3^T + \mathbf{e}_1^T)\bar{Y}_2\Gamma_7 + \mathbf{e}_1^T\bar{U}_2\} + \mathbf{e}_8^T\bar{R}_1\mathbf{e}_8\\ \bar{\mathcal{X}}_1 &= col\{\bar{X}_1\Gamma_6,\ h_M\bar{Y}_1\Gamma_6\},\ \bar{\mathcal{R}}_1 = e^{\sigma h_M}diag\{\bar{R}_1,\ 3\bar{R}_1\}\\ \bar{\mathcal{X}}_2 &= col\{\bar{X}_2\Gamma_7,\ h_M\bar{Y}_2\Gamma_7\},\ \bar{\mathcal{R}}_2 = diag\{\bar{R}_2,\ 3\bar{R}_2\}.\end{aligned}$$

In addition, the control gains are reconstructed as $F = \bar{F}\bar{G}^{-1}$ *and* $K = \bar{K}\bar{G}^{-1}$.

Proof of Lemma 1. Let us establish the congruent transformation matrixes as follows:

$$\bar{\mathbf{G}}_\kappa = I_\kappa \otimes \bar{G},\ \kappa \in \{2,3,5,8\},\ \Omega_1 = \mathrm{diag}\{\bar{\mathbf{G}}_8,\ I,\ I,\ \bar{\mathbf{G}}_2\},\ \Omega_2 = \mathrm{diag}\{\bar{G},\ I\}$$

which satisfy

$$\begin{aligned}&\Gamma_1\bar{\mathbf{G}}_8 = \bar{\mathbf{G}}_5\Gamma_1,\ \bar{\Gamma}_1\bar{\mathbf{G}}_8 = \bar{\mathbf{G}}_5\Gamma_1,\ \Gamma_2\bar{\mathbf{G}}_8 = \bar{\mathbf{G}}_2\bar{\Gamma}_2,\ \bar{\Gamma}_2\bar{\mathbf{G}}_8 = \bar{\mathbf{G}}_2\bar{\Gamma}_2,\ \Gamma_3\bar{\mathbf{G}}_8 = \bar{\mathbf{G}}_2\bar{\Gamma}_3\\ &\bar{\Gamma}_3\bar{\mathbf{G}}_8 = \bar{\mathbf{G}}_2\bar{\Gamma}_3,\ \Gamma_6\bar{\mathbf{G}}_8 = \bar{\mathbf{G}}_3\bar{\Gamma}_6, \Gamma_7\bar{\mathbf{G}}_8 = \bar{\mathbf{G}}_3\bar{\Gamma}_7, \Gamma_8\bar{\mathbf{G}}_8 = \bar{G}\Gamma_3, \mathbf{e}_p\bar{\mathbf{G}}_8 = \bar{G}\mathbf{e}_p.\end{aligned}$$

Moreover, note that (43) and (44) ensure that the matrix $\bar{G}$ is nonsingular. Then, by letting $G = \bar{G}^{-1}\Gamma_8$ and using the replacement variables listed below

$$\begin{aligned}&\bar{P} = \bar{G}^TP\bar{G},\ \bar{W}_1 = \bar{\mathbf{G}}_5^TW_1\bar{\mathbf{G}}_2,\ \bar{W}_2 = \bar{\mathbf{G}}_5^TW_2\bar{\mathbf{G}}_2,\ \bar{S}_1 = \bar{\mathbf{G}}_2^TS_1\bar{\mathbf{G}}_2,\ \bar{S}_2 = \bar{\mathbf{G}}_2^TS_2\bar{\mathbf{G}}_2\\ &\bar{S}_3 = \bar{\mathbf{G}}_2^TS_3\bar{G}^T,\ \bar{S}_4 = \bar{G}^TS_4\bar{\mathbf{G}}_2,\ \bar{S}_5 = \bar{G}^TS_5\bar{G}^T,\ \bar{R}_1 = \bar{G}^TR_1\bar{G},\ \bar{X}_1 = \bar{G}^TX_1\bar{\mathbf{G}}_3\\ &\bar{Y}_1 = \bar{G}^TX_1\bar{\mathbf{G}}_3,\ \bar{R}_2 = \bar{G}^TR_2\bar{G},\ \bar{X}_2 = \bar{G}^TX_2\bar{\mathbf{G}}_3,\ \bar{Y}_2 = \bar{G}^TX_2\bar{\mathbf{G}}_3,\ \bar{U}_1 = \bar{G}^TU_1\bar{\mathbf{G}}_8\\ &\bar{U}_2 = \bar{G}^TU_2\bar{\mathbf{G}}_8,\ \bar{F} = F\bar{G},\ \bar{K} = K\bar{G}\end{aligned}$$

we can obtain

$$\begin{aligned}&\bar{\mathbf{G}}_8^T\Psi_i^*\bar{\mathbf{G}}_8 = \bar{\Psi}_i^*,\ \bar{\mathbf{G}}_8^T\Psi_0\bar{\mathbf{G}}_8 = \bar{\Psi}_0,\ \bar{\mathbf{G}}_8^T\Psi_1\bar{\mathbf{G}}_8 = \bar{\Psi}_1\\ &\bar{\mathbf{G}}_8^T\Psi_2\bar{\mathbf{G}}_8 = \bar{\Psi}_2,\ \bar{\mathbf{G}}_2^T\mathcal{X}_q\bar{\mathbf{G}}_8 = \bar{\mathcal{X}}_q,\ \bar{\mathbf{G}}_2^T\mathcal{R}_q\bar{\mathbf{G}}_2 = \bar{\mathcal{R}}_q.\end{aligned}$$

Thus, pre- and postmultiplying (19) by Ω_1^T and Ω_1 yields (42), and pre- and postmultiplying (20) by Ω_2^T and Ω_2 yields (43).

In parallel, to scale the size of the DoA, let us employ an additional ellipsoid $\mathcal{E}(P_0,1)$ satisfying that $\mathcal{E}(P_0,1) \subset \mathcal{E}(P,1)$, i.e.,

$$\bar{G}^TP_0\bar{G} \geq \bar{G}^TP\bar{G} = \bar{P}. \tag{45}$$

Indeed, since it holds that $\bar{G}^TP_0\bar{G} \geq \mathrm{He}\{\mu\bar{G}\} - \mu^2P_0^{-1}$, condition (45) is ensured by

$$0 \leq \mathrm{He}\{\mu\bar{G}\} - \mu^2P_0^{-1} - \bar{P}$$

which is transformed to (44) by the Schur complement. □

Remark 5. *The DoA* $\mathcal{E}(P,1)$ *can be enlarged by the following LMI solver programming:* min *trace*(P_0) *such that LMIs (42)–(44) hold.*

4. Numerical Validation

In this section, we utilize Corollary 1 to obtain comparative stability analysis results for three linear systems. Additionally, we utilize the stabilization criteria derived in Theorem 1 to design a sampled-data controller for a linearized IPS.

4.1. Comparison Examples

Let us consider three sampled-data linear systems, used in [8,9,15]:

$$\text{System 1: } \left[\begin{array}{c|c} A & A_s \end{array}\right] = \left[\begin{array}{cc|cc} -1 & 0 & -1 & 1 \\ 1 & -2 & 1 & 0 \end{array}\right] \tag{46}$$

$$\text{System 2: } \left[\begin{array}{c|c} A & A_s \end{array}\right] = \left[\begin{array}{cc|cc} -2 & 0 & -1 & 0 \\ 0 & -0.9 & -1 & -1 \end{array}\right] \tag{47}$$

$$\text{System 3: } \left[\begin{array}{c|c} A & A_s \end{array}\right] = \left[\begin{array}{cc|cc} -1 & -1 & 0 & 0 \\ -1 & -2 & -1 & -2 \end{array}\right]. \tag{48}$$

For systems (46)–(48) and $h_m = 10^{-5}$, Table 1 lists the maximum upper bound of the sampling interval h_M^* obtained by Theorem 4 in [7], Theorem 1 in [8], Corollary 1 in [9], Theorem 3 in [15], Theorem 2 in [26], and Corollary 1 with $\sigma = 0.1$. As compared in Table 1, the proposed method offers a longer sampling interval for each system than [8,9,15] despite requiring a lower computational complexity.

Table 1. Maximum upper bound of sampling interval for $h_m = 10^{-5}$.

Methods	System 1	System 2	System 3	NoVs
Theorem 2 in [26]	2.2236	2.8554	2.1881	156
Theorem 4 in [7]	3.9306	3.2632	6.2279	263
Theorem 3 in [15]	–	3.2660	–	455
Theorem 1 in [8]	5.3040	–	–	475
Corrollary 1 in [9]	–	3.2672	6.3373	291
Corollary 1	6.7461	3.2696	7.8603	285

4.2. Application to Inverted Pendulum System

Let us consider the IPS shown in Figure 2, where $x_c(t)$ is the cart position, $\theta(t)$ is the pendulum angle, $F_c(t)$ is the force applied to the cart to keep the pendulum stable around the equilibrium position, and $w(t)$ indicates the exogenous disturbances due to friction. To be specific, the IPS parameters and their numerical values are listed in Table 2. As in [27], the motion dynamics of the inverted pendulum are given by

$$(J_{eq} + M)\ddot{x}_c(t) + Ml\cos(\theta)\ddot{\theta}(t) - Ml\sin(\theta(t))\dot{\theta}^2(t) = F_c(t) - D_{eq}\dot{x}_c(t) - w(t) \tag{49}$$

$$Ml\cos(\theta)\ddot{x}_c(t) + (J + Ml^2)\ddot{\theta}(t) + Mlg\sin(\theta(t)) = -D\dot{\theta}(t) + 0.01w(t) \tag{50}$$

where the force $F_c(t)$ is described as follows:

$$F_c(t) = \frac{LN_t}{Rr}\left(-\frac{LN\dot{x}_c(t)}{r} + u(t)\right) \tag{51}$$

in which $u(t)$ indicates the voltage control input applied to the cart motor. Then, by letting $x_1(t) = x_c(t)$, $x_2(t) = \theta(t)$, $x_3(t) = \dot{x}_c(t)$, and $x_4(t) = \dot{\theta}(t)$, the linearized model around the equilibrium position, i.e., $\sin(\theta(t)) \cong \theta(t)$, $\cos(\theta(t)) \cong 1$, and $\dot{\theta}^2(t) \cong 0$, is derived from (49)–(51) as follows:

$$\begin{cases} \dot{x}(t) = Ax(t) + Bu(t) + Ew(t) \\ z(t) = Cx(t) \end{cases} \tag{52}$$

where

$$A = \begin{bmatrix} 0 & 0 & 1 & 0 \\ 0 & 0 & 0 & 1 \\ 0 & A_{32} & A_{33} & A_{34} \\ 0 & A_{42} & A_{43} & A_{44} \end{bmatrix}, \; B = \begin{bmatrix} 0 \\ 0 \\ B_{31} \\ B_{41} \end{bmatrix}$$

$$C = \begin{bmatrix} 1 & 0 & 0 & 0 \\ 0 & 1 & 0 & 0 \end{bmatrix}, \; E = \begin{bmatrix} 0 & 0 & E_{31} & E_{41} \end{bmatrix}^T$$

in which

$$A_{32} = \frac{M^2 l^2 g}{J_t},\ A_{33} = -\frac{(J + Ml^2)D_{eq}}{J_t} - \frac{L^2 N_t N (J + Ml^2)}{Rr^2 J_t},\ A_{34} = -\frac{MlD}{J_t}$$
$$A_{42} = \frac{(J_{eq} + M)Mlg}{J_t},\ A_{43} = -\frac{MlD_{eq}}{J_t} - \frac{L^2 N_t N Ml}{Rr^2 J_t},\ A_{44} = -\frac{(J_{eq} + M)D}{J_t}$$
$$B_{31} = \frac{LN_t(J + Ml^2)}{RrJ_t},\ B_{41} = \frac{LN_t Ml}{RrJ_t},\ E_{31} = -\frac{(J + Ml^2)}{J_t}$$
$$E_{41} = \frac{0.01(J_{eq} + M)}{J_t},\ J_t = (J_{eq} + M)J + J_{eq}Ml^2.$$

Let us recall (52) subject to $\bar{u} = 10$ and $\bar{w} = 0.45$. Then, Theorem 1 with $\chi_1 = 1$, $\chi_2 = 3.5, \sigma = 1, \mu = 15$ offers $h_M^* = 0.205$ (s) as the maximum upper bound of the sampling interval with respect to $h_m = 0.001$ (s). Furthermore, Figure 3 shows the minimum peak-to-peak performance level that varies according to the upper bound of sampling interval and the saturation level. It can be found from Figure 3 that the peak-to-peak performance deteriorates as the upper bound of the sampling interval increases and the saturation level decreases. In particular, $\gamma_{\min}$ is rapidly increased when the value of h_M increases from 0.175 (s) to 0.205 (s). Specifically, for the following three cases:

$$\begin{aligned}&\text{Case 1: } h_M = 0.01(s) \text{ and } \gamma = 1.6332\\ &\text{Case 2: } h_M = 0.10(s) \text{ and } \gamma = 2.3920\\ &\text{Case 3: } h_M = 0.175(s) \text{ and } \gamma = 4.6247\end{aligned}$$

Remark 5 provides

$$\begin{aligned}&\text{Case 1 :}\\ &F = \begin{bmatrix} 5.5852 & -30.1195 & 12.8607 & -4.3882 \end{bmatrix}\\ &K = \begin{bmatrix} 5.4639 & -29.6907 & 12.6716 & -4.3251 \end{bmatrix}\\ &P = \begin{bmatrix} 4.5780 & -5.2386 & 2.5633 & -0.7720 \\ -5.2386 & 14.1654 & -6.1937 & 2.0509 \\ 2.5633 & -6.1937 & 2.7860 & -0.9095 \\ -0.7720 & 2.0509 & -0.9095 & 0.3002 \end{bmatrix}\\ &\text{Case 2 :}\\ &F = \begin{bmatrix} 4.1453 & -28.4985 & 12.0733 & -4.1541 \end{bmatrix}\\ &K = \begin{bmatrix} 4.1437 & -28.4934 & 12.0710 & -4.1534 \end{bmatrix}\\ &P = \begin{bmatrix} 4.9204 & -5.7146 & 2.7923 & -0.8423 \\ -5.7146 & 15.5514 & -6.8186 & 2.2565 \\ 2.7923 & -6.8186 & 3.0696 & -1.0024 \\ -0.8423 & 2.2565 & -1.0024 & 0.3308 \end{bmatrix}\\ &\text{Case 3 :}\\ &F = \begin{bmatrix} 2.7485 & -25.8155 & 10.8558 & -3.7652 \end{bmatrix}\\ &K = \begin{bmatrix} 2.7485 & -25.8155 & 10.8558 & -3.7652 \end{bmatrix}\\ &P = \begin{bmatrix} 6.1112 & -7.1130 & 3.4783 & -1.0485 \\ -7.1130 & 18.5068 & -8.1869 & 2.6947 \\ 3.4783 & -8.1869 & 3.7047 & -1.2050 \\ -1.0485 & 2.6947 & -1.2050 & 0.3957 \end{bmatrix}.\end{aligned} \tag{53}$$
$$\tag{54}$$
$$\tag{55}$$

Table 2. Inverted pendulum system parameters [27].

Description	Symbol	Value
Cart mass	M_c	0.94 kg
Pendulum mass	M	0.1270 kg
Pendulum length	l	0.1778 m
Pendulum moment of inertia	J	0.0012 N/m
Lumped mass of the cart	J_{eq}	1.0731 kg
Viscous damping coefficient	D	0.0024 N s/m
Motor viscous damping	D_{eq}	5.40 N s/m
Motor back-EMF constant	N	0.0077 V s/rad
Motor torque constant	N_t	0.0077 Nm/A
Gearbox gear ratio	L	3.71
Motor armature resistance	R	2.60 Ω
Motor pinion radius	r	0.0064 m
Gravity constant	g	9.81 m/s^2

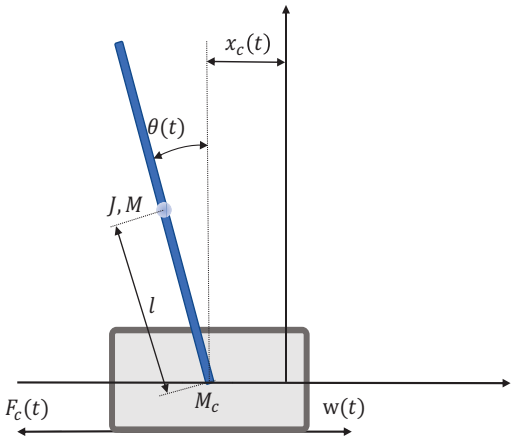

Figure 2. Diagram of inverted pendulum system.

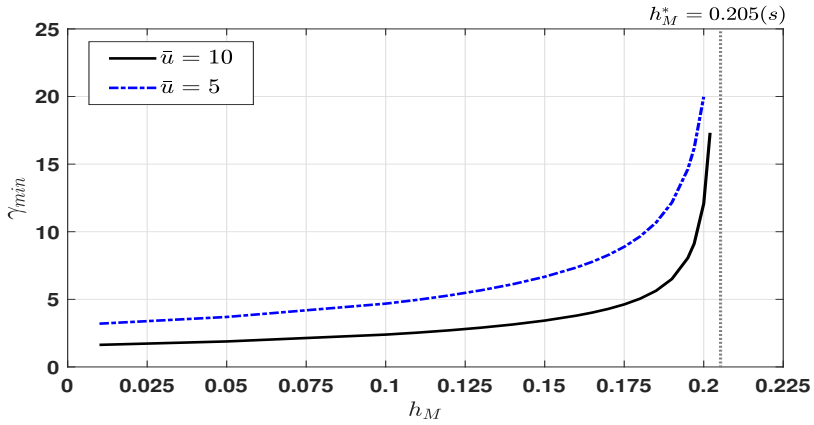

Figure 3. Minimum peak-to-peak performance level for h_M and $\bar{u}$.

Based on (53)–(55), Figure 4 plots the state trajectory starting at $x_c(t_0) = 0.0$ (mm) and $\theta(t_0) = 5$(deg) for each case, where the exogenous disturbance is given by $w(t) = 0.45 \times \sin(1.66\pi t)$. As can be seen from Figure 4, the size of DoA $\mathcal{E}(P, 1)$ becomes smaller and the range of the state trajectory widens as h_M increases from 0.01 (s) to 0.175 (s).

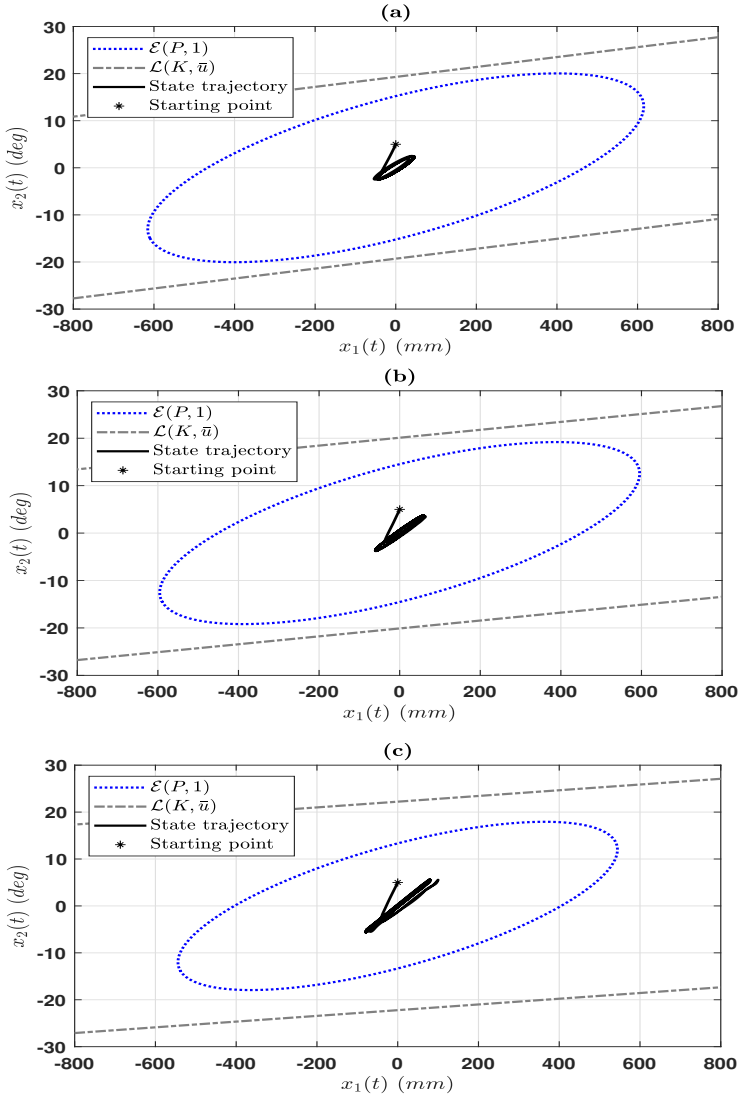

Figure 4. Simulation results: DoA $\mathcal{E}(P,1)$ and state trajectory for three cases: (**a**) $h_M = 0.01$ (s), (**b**) $h_M = 0.10$ (s), and (**c**) $h_M = 0.175$ (s).

Subsequently, the block diagram and laboratory setup for experimental verification are depicted in Figure 5 (IP02 Linear Inverted Pendulum, Quanser Inc., 119 Spy Court, Markham, ON L3R 5H6, Canada), where a cart is driven by a Faulhaber Coreless DC Motor (2338S006) connected to a Faulhaber Planetary Gearhead Series 23/1; the cart position and the pendulum angle are measured using a quadrature incremental encoder; and the amplifier (VoltPAQ-X1) is used to amplify the control input to the motor voltage. At each sampling time, the cart position and pendulum angle are sampled and transferred to the controller embedded in the MyRIO instrument. Subsequently, the control input $u(t)$ is generated according to the state-feedback control law given in (4) and then transferred to the VoltPAQ amplifier with the saturation level $\pm$ 10 (V). Ultimately, using the amplified voltage control input, the cart motor generates the force to balance the pendulum. Practically, based on (53)–(55), Figure 6 shows the experimental state trajectory starting at $x_c(t_0) = 0.0(mm)$ and $\theta(t_0) = 5(deg)$ for each case, which illustrates that the proposed method has a suitable ability to stabilize system (52) in the DoA.

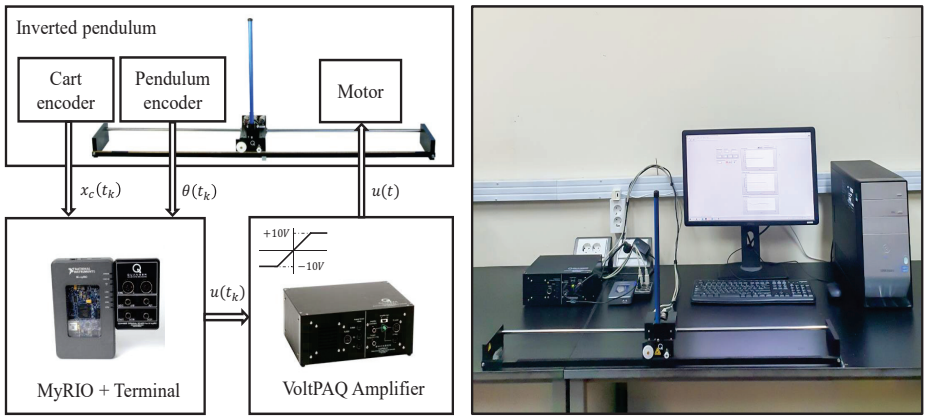

Figure 5. Block diagram and laboratory setup.

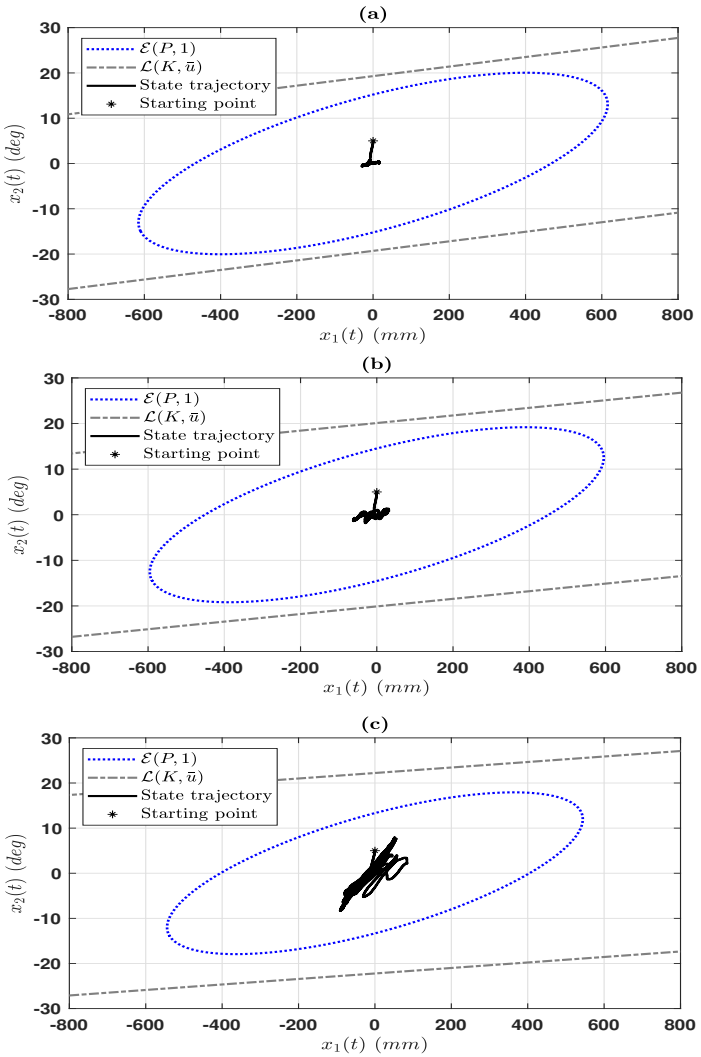

Figure 6. Experiment results: DoA $\mathcal{E}(P,1)$ and state trajectory for three cases: (**a**) $h_M = 0.01$ (s), (**b**) $h_M = 0.10$ (s), and (**c**) $h_M = 0.175$ (s).

In particular, for $h_M = 0.175$ (s), Figure 7a–c present the cart position, the pendulum angle, and the voltage control input, where $w(t) = 0.45 \times \sin(1.66\pi t)$ is used as the exogenous disturbance acting on this control system. As shown in Figure 7a,b, the cart position and the pendulum angle are continuously affected by $w(t)$ but operate stably

within the allowable range. Also, from Figure 7c, it can be observed that the sampled-data voltage control input is generated subject to the saturation constraint $\bar{u} = 10$.

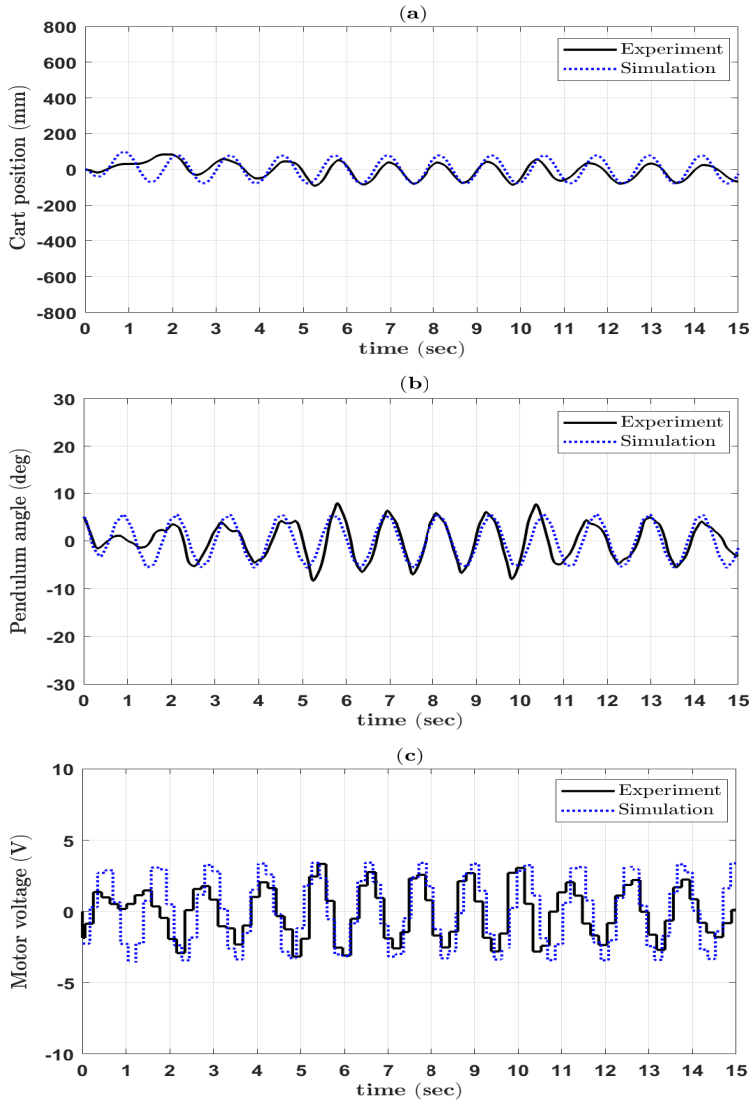

Figure 7. System state response and sampled-data control input.

Finally, for $x(t_0) = 0$ and $w(t) = 0.45 \times \sin(1.66\pi t)$, i.e., $||w(t)||_\infty^2 = 0.2025$, Figure 8a,b display the experimental performance output of (52) and its squared Euclidean norm, respectively, which demonstrates that the practical peak-to-peak performance satisfies

$$\frac{||z(t)||_\infty^2}{||w(t)||_\infty^2} < \frac{0.05}{0.2025} < \gamma^2 = 4.6247^2.$$

Remark 6. *It should be noted that the linearized model (52) is developed under the assumption that there is no uncertainty in the system parameters. This assumption can create a gap between the mathematical model and the actual dynamic system, resulting in some errors between experimental and simulation results. To overcome this limitation, our future research will focus on developing robust T-S fuzzy control systems and multidimensional quasi-linear control systems.*

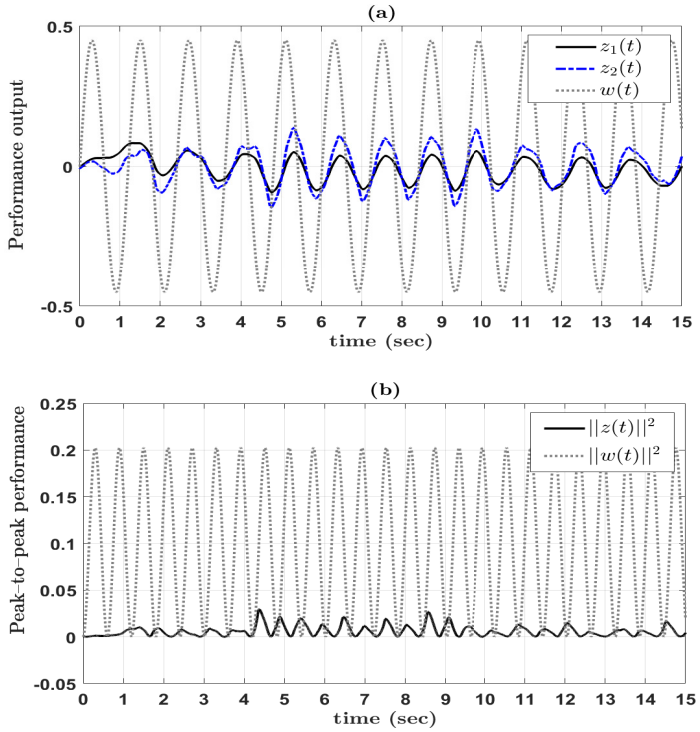

Figure 8. Experiment results: (**a**) performance output $z(t)$, and (**b**) peak-to-peak performance.

5. Conclusions

This paper has proposed a method for designing an improved sampled-data controller for continuous-time linear systems with actuator saturation and peak-bounded exogenous disturbances. To be specific, two novel time integrals of the weighted state derivative have been introduced to construct an improved looped-functional. In addition, two additional zero-equalities have been utilized to obtain less conservative stability analysis criteria. Following that, a set of LMIs-based stabilization conditions has been developed to ensure that the closed-loop system achieves exponential stability with a guaranteed peak-to-peak performance in the DoA. Compared to other existing studies, the proposed method not only offers an improved maximum upper bound of sampling interval but also requires lower computational complexity. Finally, the effectiveness of the proposed method has been demonstrated through its successful implementation in an IPS.

Author Contributions: Conceptualization, S.H.K.; Data curation, K.H.N. and S.H.K.; Formal analysis, K.H.N. and S.H.K.; Funding acquisition, S.H.K.; Investigation, S.H.K.; Methodology, K.H.N. and S.H.K.; Project administration, S.H.K.; Resources, S.H.K.; Software, K.H.N.; Supervision, S.H.K.; Validation, K.H.N. and S.H.K.; Visualization, K.H.N. and S.H.K.; Writing—original draft, K.H.N. and S.H.K.; Writing—review & editing, K.H.N. and S.H.K. All authors have read and agreed to the published version of the manuscript.

Funding: This work was supported by the National Research Foundation of Korea Grant funded by the Korean Government (NRF-2023R1A2C1002635). This results was supported by "Regional Innovation Strategy(RIS)" through the National Research Foundation of Korea (NRF) funded by the Ministry of Education (MOE) (2021RIS-003).

Data Availability Statement: The authors confirm that the data supporting the findings of this study are available within the article.

Conflicts of Interest: The authors declare no conflict of interest.

References

1. Lee, T.H.; Park, J.H. New methods of fuzzy sampled-data control for stabilization of chaotic systems. *IEEE Trans. Syst. Man Cybern.-Syst.* **2017**, *48*, 2026–2034. [CrossRef]
2. Lv, X.; Li, X. Finite time stability and controller design for nonlinear impulsive sampled-data systems with applications. *ISA Trans.* **2017**, *70*, 30–36. [CrossRef] [PubMed]
3. Nguyen, K.H.; Kim, S.H. Improved sampled-data control design of T-S fuzzy systems against mismatched fuzzy-basis functions. *Appl. Math. Comput.* **2022**, *428*, 127150. [CrossRef]
4. Nguyen, K.H.; Kim, S.H. Improved stability and stabilization criteria of sampled-data control systems based on an improved looped-functional. *Math. Comput. Simul.* **2024**, *215*, 69–81. [CrossRef]
5. Fridman, E.; Seuret, A.; Richard, J.-P. Robust sampled-data stabilization of linear systems: An input delay approach. *Automatica* **2004**, *40*, 1441–1446. [CrossRef]
6. Seuret, A. A novel stability analysis of linear systems under asynchronous samplings. *Automatica* **2012**, *48*, 177–182. [CrossRef]
7. Zeng, H.-B.; Teo, K.L.; He, Y. A new looped-functional for stability analysis of sampled-data systems. *Automatica* **2017**, *82*, 328–331. [CrossRef]
8. Wang, X.; Sun, J.; Dou, L. Improved results on stability analysis of sampled-data systems. *Int. J. Robust Nonlinear Control* **2021**, *31*, 6549–6561. [CrossRef]
9. Sheng, Z.; Lin, C.; Chen, B.; Wang, Q.-G. Stability analysis of sampled-data systems via novel Lyapunov functional method. *Inf. Sci.* **2022**, *585*, 559–570. [CrossRef]
10. Sugihara, T.; Nakamura, Y.; Inoue, H. Real-time humanoid motion generation through ZMP manipulation based on inverted pendulum control. *IEEE Int. Conf. Robot. Autom.* **2002**, *2*, 1404–1409.
11. Li, Z.; Yang, C. Neural-adaptive output feedback control of a class of transportation vehicles based on wheeled inverted pendulum models. *IEEE Trans. Control Syst. Technol.* **2011**, *20*, 1583–1591. [CrossRef]
12. El-Bardini, M.; El-Nagar, A. Interval type-2 fuzzy PID controller for uncertain nonlinear inverted pendulum system. *ISA Trans.* **2014**, *53*, 732–743. [CrossRef] [PubMed]
13. Lee, H.; Gil, J.; You, S.; Gui, Y.; Kim, W. Arm angle tracking control with pole balancing using equivalent input disturbance rejection for a rotational inverted pendulum. *Mathematics* **2021**, *9*, 2745. [CrossRef]
14. Saleem, O.; Abbas, F.; Iqbal, J. Complex fractional-order LQIR for inverted-pendulum-type robotic mechanisms: Design and experimental validation. *Mathematics* **2023**, *11*, 913. [CrossRef]
15. Lee, S.-H.; Selvaraj, P.; Park, M.-J.; Kwon, O.-M. Improved results on $\mathcal{H}_\infty$ stability analysis of sampled-data systems via looped-functionals and zero equalities. *Appl. Math. Comput.* **2020**, *373*, 125003. [CrossRef]
16. Nguyen, K.H.; Kim, S.H. Event-triggered Non-PDC filter design of fuzzy Markovian jump systems under mismatch phenomena. *Mathematics* **2022**, *10*, 2917. [CrossRef]
17. Gao, Z.-M.; He, Y.; Liu, G.-P. New results on stability and $\mathcal{H}_\infty$ performance analysis for aperiodic sampled-data systems via augmented Lyapunov functional. *ISA Trans.* **2022**, *128*, 309–315. [CrossRef]
18. Nguyen, K.H.; Kim, S.H. Improved dissipativity-based sampled-data control synthesis of nonhomogeneous Markovian jump fuzzy systems against mismatched fuzzy-basis functions. *Inf. Sci.* **2022**, *607*, 1439–1464. [CrossRef]
19. Abedor, J.; Nagpal, K.; Poolla, K. A linear matrix inequality approach to peak-to-peak gain minimization. *Int. J. Robust Nonlinear Control* **1996**, *6*, 899–927. [CrossRef]
20. Ahn, C.K.; Shi, P.; Basin, M.V. Two-dimensional peak-to-peak filtering for stochastic Fornasini–Marchesini systems. *IEEE Trans. Autom. Control* **2017**, *63*, 1472–1479. [CrossRef]
21. Zeng, H.-B.; Teo, K.L.; He, Y.; Xu, H.; Wang, W. Sampled-data synchronization control for chaotic neural networks subject to actuator saturation. *Neurocomputing* **2017**, *260*, 25–31. [CrossRef]
22. Yan, Z.; Huang, X.; Liang, J. Aperiodic sampled-data control for stabilization of memristive neural networks with actuator saturation: A dynamic partitioning method. *IEEE Trans. Cybern.* **2021**, *53*, 1725–1737. [CrossRef]
23. Fan, Y.; Huang, X.; Li, Y. Aperiodic sampled-data control for local stabilization of memristive neural networks subject to actuator saturation: Discrete-time Lyapunov approach. *ISA Trans.* **2022**, *127*, 361–369. [CrossRef] [PubMed]
24. Kwon, W.; Park, J. Improved criteria of sampled-data master-slave synchronization for chaotic neural networks with actuator saturation. *J. Frankl. Inst.* **2023**, *360*, 5134–5148. [CrossRef]
25. Hu, T.; Lin, Z.; Chen, B.M. An analysis and design method for linear systems subject to actuator saturation and disturbance. *Automatica* **2002**, *38*, 351–359. [CrossRef]
26. Lee, T.H.; Park, J.H. Stability analysis of sampled-data systems via free-matrix-based time-dependent discontinuous Lyapunov approach. *IEEE Trans. Autom. Control* **2017**, *62*, 3653–3657. [CrossRef]
27. Blondin, M.J.; Pardalos, P.M. A holistic optimization approach for inverted cart-pendulum control tuning. *Soft Comput.* **2020**, *24*, 4343–4359. [CrossRef]